Supporting Information for "Dynamical Signatures from Competing, Nonadiabatic Fragmentation Pathways of *S*-Nitrosothiophenol"

K. Jacob Blackshaw,[1] Marcus Marracci,[2] Robert T. Korb,[1] Naa-Kwarley Quartey,[1] Annalise K. Ajmani,[1] David J. Hood,[1] Christopher J. Abelt,[1] Belinda I. Ortega,[2] Kate Luong[2], Andrew S. Petit,*[,2] Nathanael M. Kidwell*[,1]

[1]*Department of Chemistry, The College of William and Mary, Williamsburg, VA 23187-8795, USA*

[2] *Department of Chemistry and Biochemistry, California State University – Fullerton, Fullerton, CA 92834-6866, USA*

* Authors to whom correspondence should be addressed. E-mail: nmkidwell@wm.edu; apetit@fullerton.edu

Table of Contents

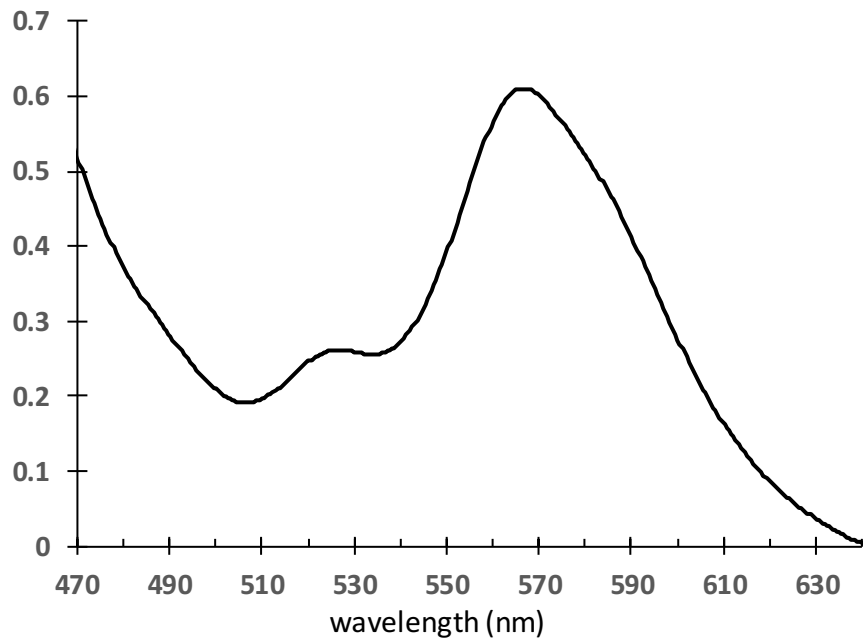

Figure S1: Electronic absorption spectrum of PhSNO in CH_2Cl_2. This spectrum was generated by reaction of PhSH (0.045 **M** in CH_2Cl_2) with N_2O_4/Norit (0.2 g) at 0°C for 40 min. The absorbance of 0.61 at 570 nm (ε = 53 $\mathbf{M}^{-1}cm^{-1}$)[§] indicates a 26% conversion.

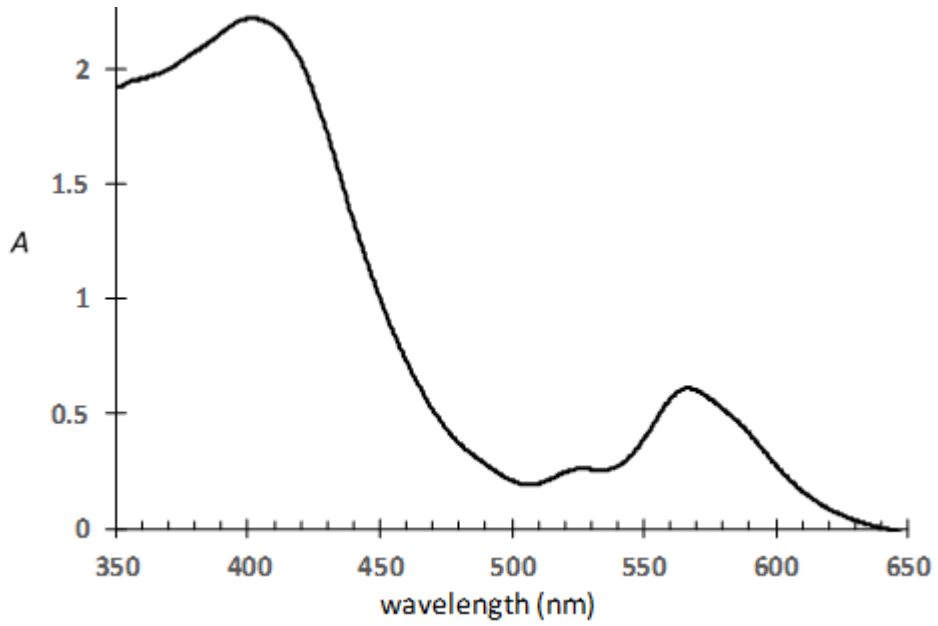

Figure S2: Electronic absorption spectrum of PhSNO in CH_2Cl_2 (above) showing the short wavelength region. This region also contains absorptions from PhSH and PhSSPh.

[§]Zolfigol, M. A.; Shirini, F.; Choghamarani, A. G.; Ghofrani, E. Silica Chloride/$NaNO_2$ as a Novel Heterogeneous System for Production of Thionitrites and Disulfides Under Mild Conditions *Phosphorus, Sulfur, and Silicon and the Related Elements* **2003**, *178*, 1477-1481.

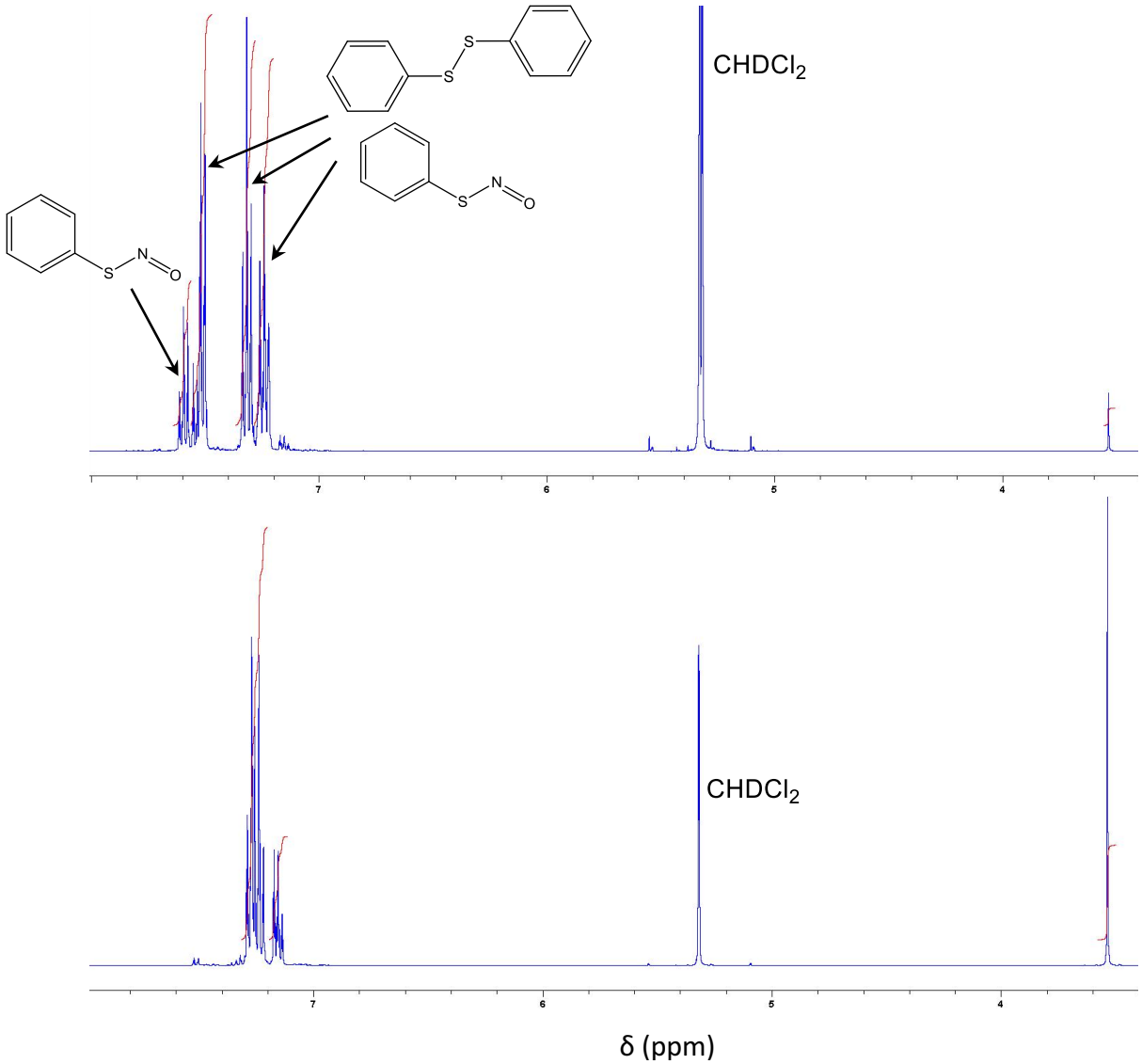

Figure S3: ^{1}H NMR (400 MHz, CD_2Cl_2) of PhSH (0.09 **M**, bottom) and after reacting with N_2O_4/Norit (0.4 g) for 49 min at 0°C (top). The conversion is 93% and the yield of PhSNO is 29% by integration.

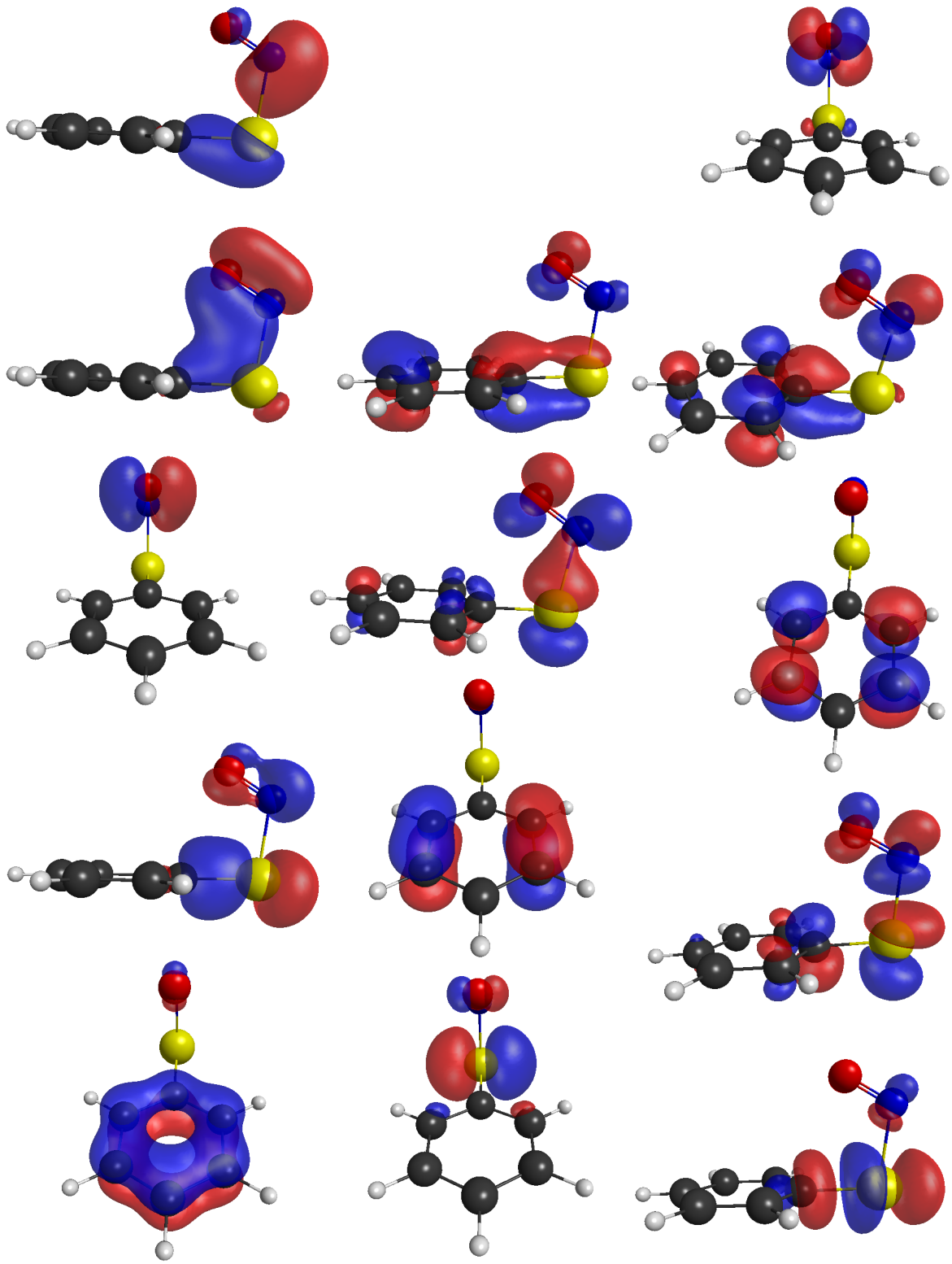

Figure S4: The (18,14) active space used in the relaxed scan along the S-N bond dissociation coordinate. The molecular orbitals in the first two columns are doubly occupied in the Hartree-Fock ground state whereas those in the last column are virtual.

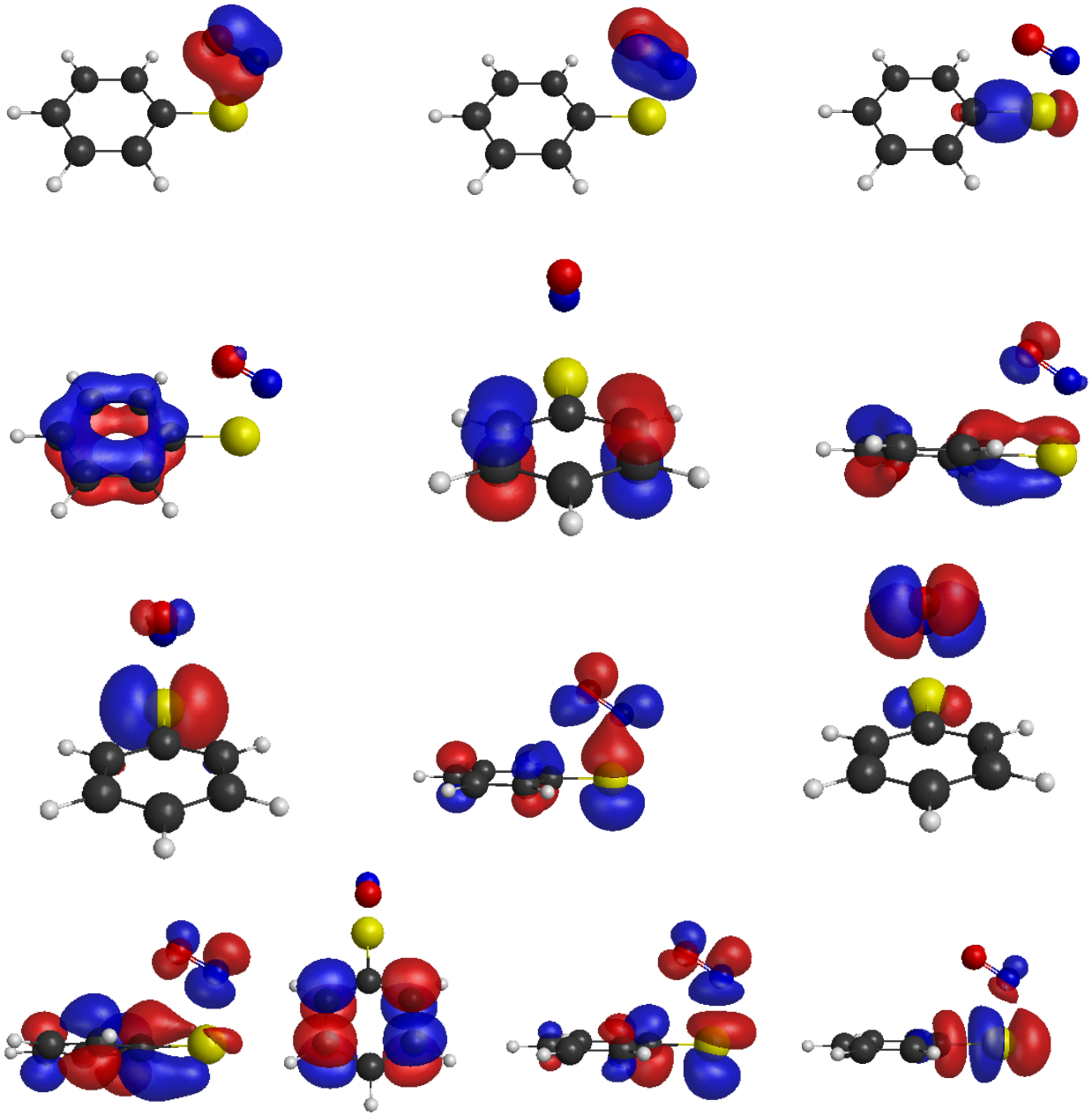

Figure S5: The (16,13) active space used in the torsion scan at $R_{S\text{-}N}$ = 1.9Å and a C-S-N-O torsion angle of 0º. Reading from left to right and top to bottom, the first eight molecular orbitals are doubly occupied in the Hartree-Fock ground state whereas the final five molecular oarbitals are virtual.

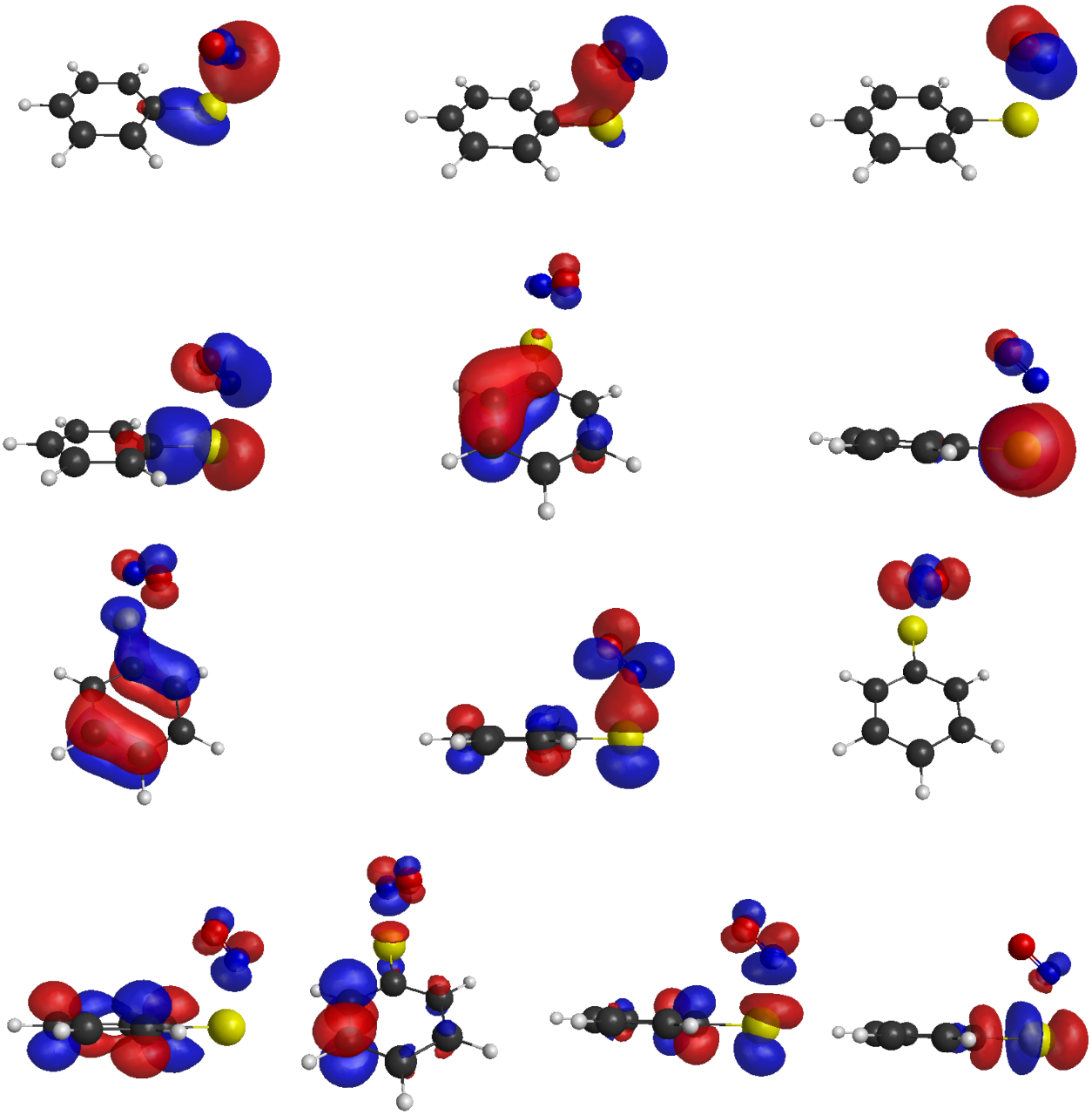

Figure S6: The (16,13) active space used in the torsion scan at $R_{S\text{-}N}$ = 1.9Å and a C-S-N-O torsion angle of 30º. Reading from left to right and top to bottom, the first eight molecular orbitals are doubly occupied in the Hartree-Fock ground state whereas the final five molecular oarbitals are virtual.

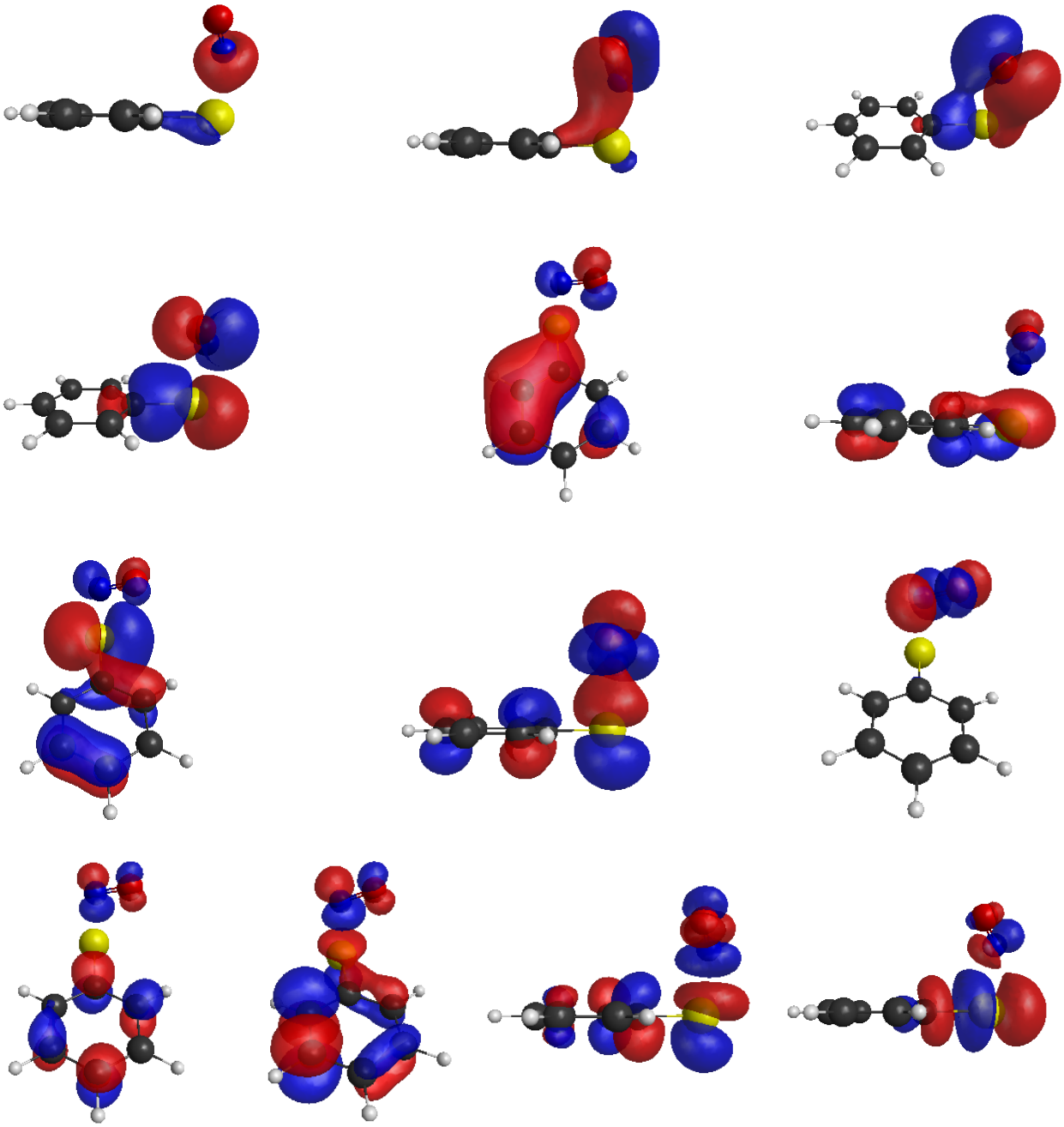

Figure S7: The (16,13) active space used in the torsion scan at $R_{S\text{-}N}$ = 1.9Å and a C-S-N-O torsion angle of 60º. Reading from left to right and top to bottom, the first eight molecular orbitals are doubly occupied in the Hartree-Fock ground state whereas the final five molecular oarbitals are virtual.

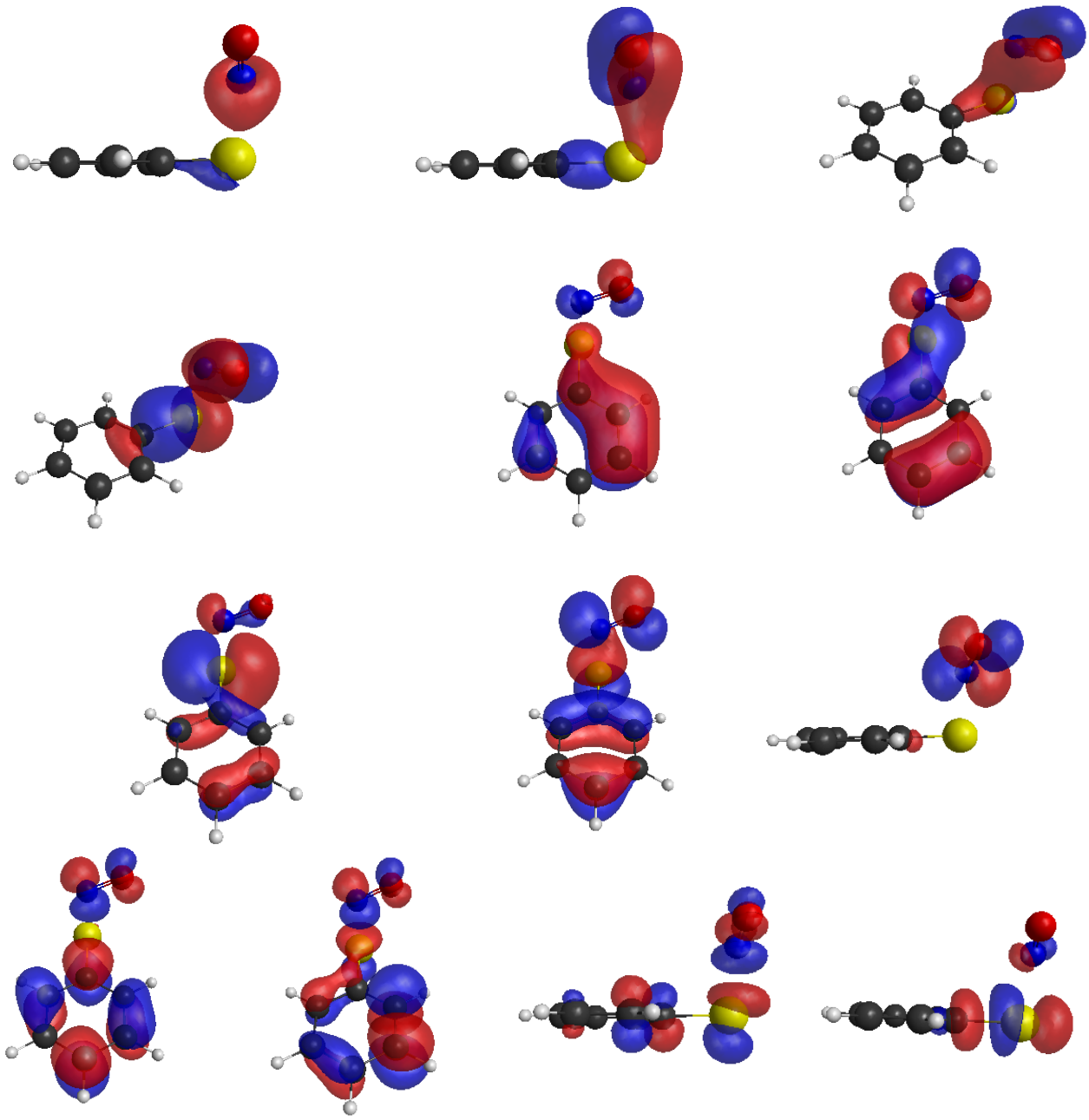

Figure S8: The (16,13) active space used in the torsion scan at $R_{S\text{-}N}$ = 1.9Å and a C-S-N-O torsion angle of 90º. Reading from left to right and top to bottom, the first eight molecular orbitals are doubly occupied in the Hartree-Fock ground state whereas the final five molecular oarbitals are virtual.

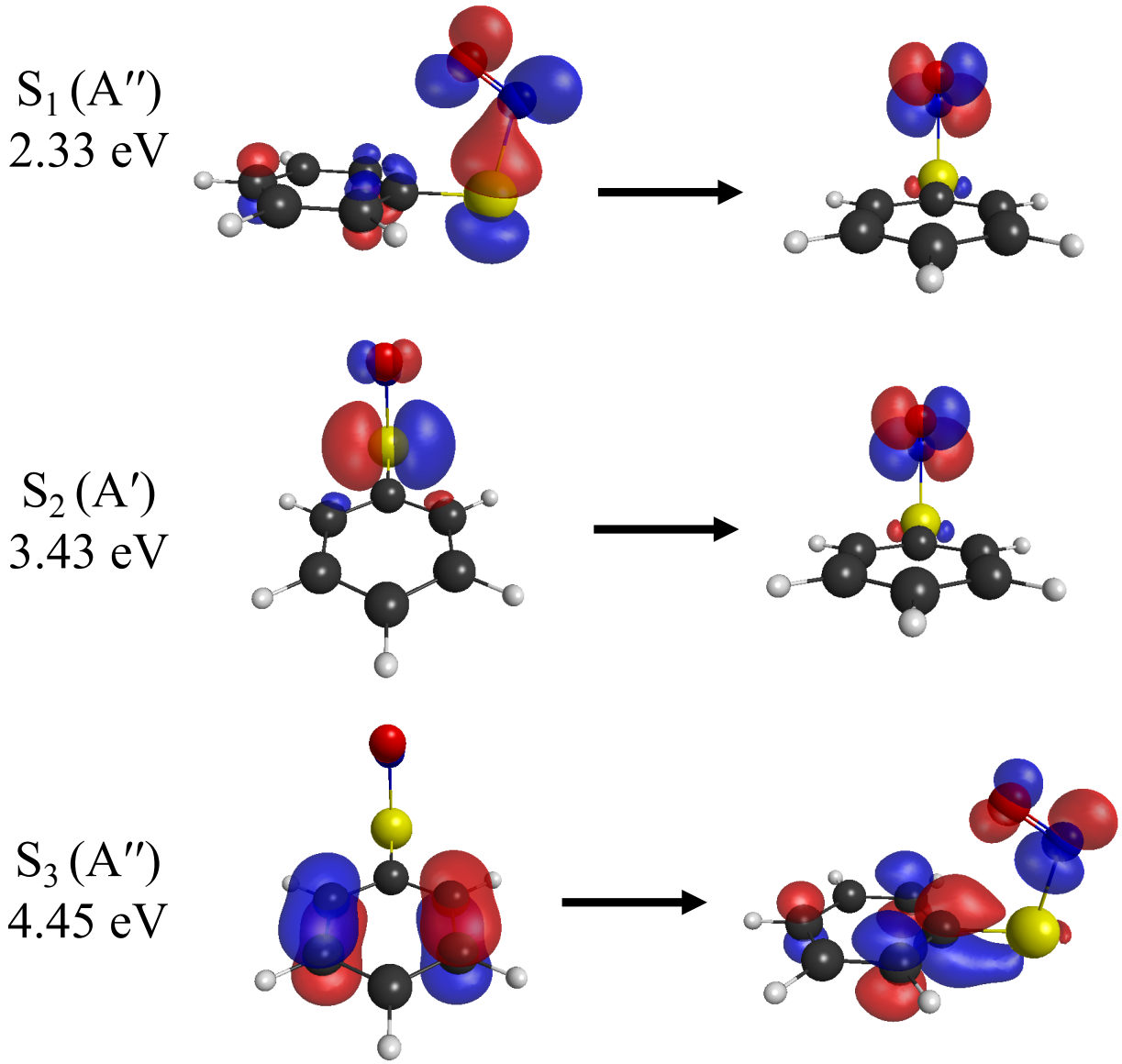

Figure S9: The dominant molecular orbitals associated with the $S_0 \rightarrow S_1$, $S_0 \rightarrow S_2$, and $S_0 \rightarrow S_3$ transitions at the optimized geometry of the *syn* conformer along with the vertical excitation energies calculated at the (18,14) MCQDPT2/aug-cc-pVDZ level of theory.

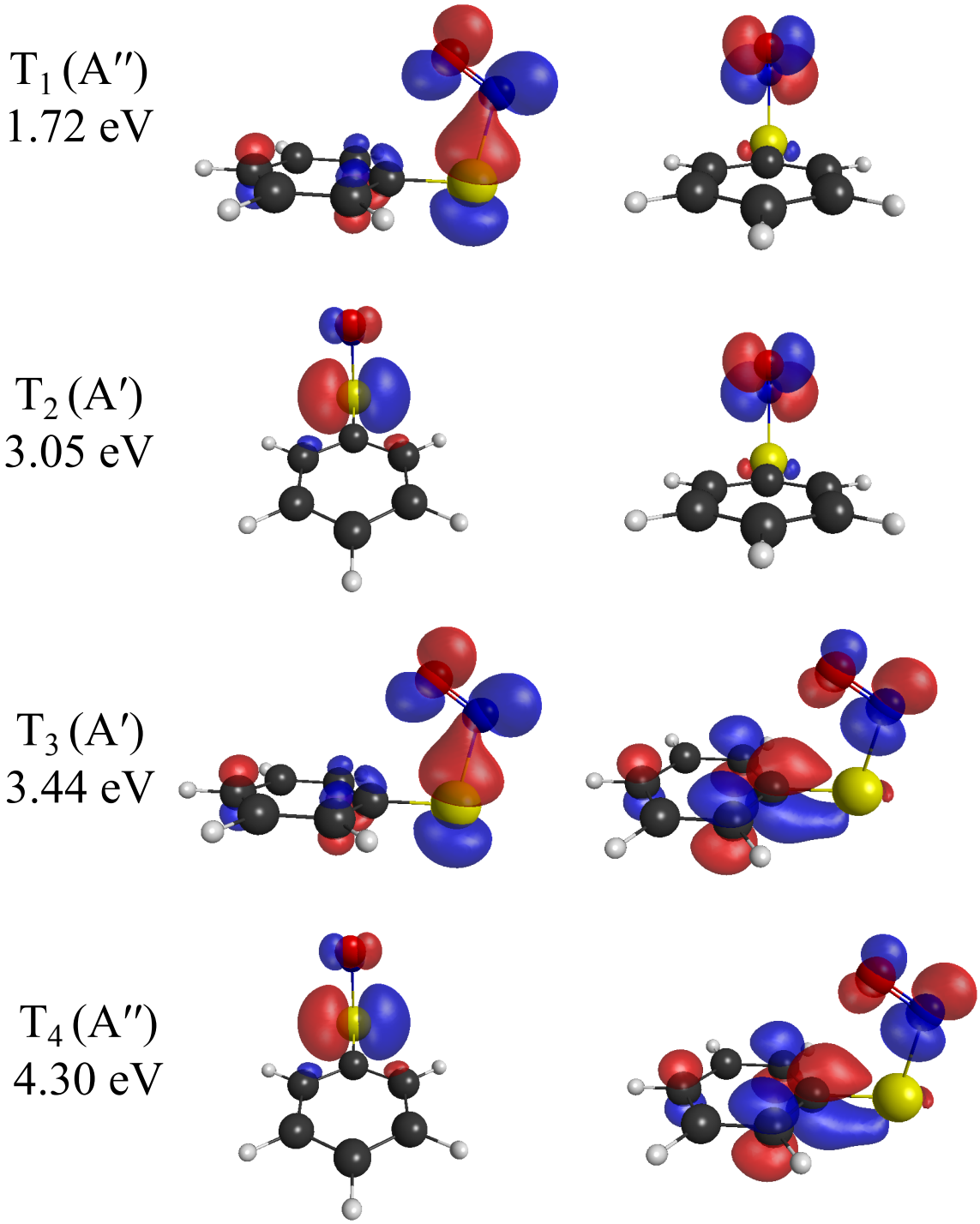

Figure S10: The singly occupied molecular orbitals in the dominant electron configurations of the T_1, T_2, T_3, and T_4 states at the optimized geometry of the *syn* conformer along with the vertical excitation energies calculated at the (18,14) MCQDPT2/aug-cc-pVDZ level of theory.

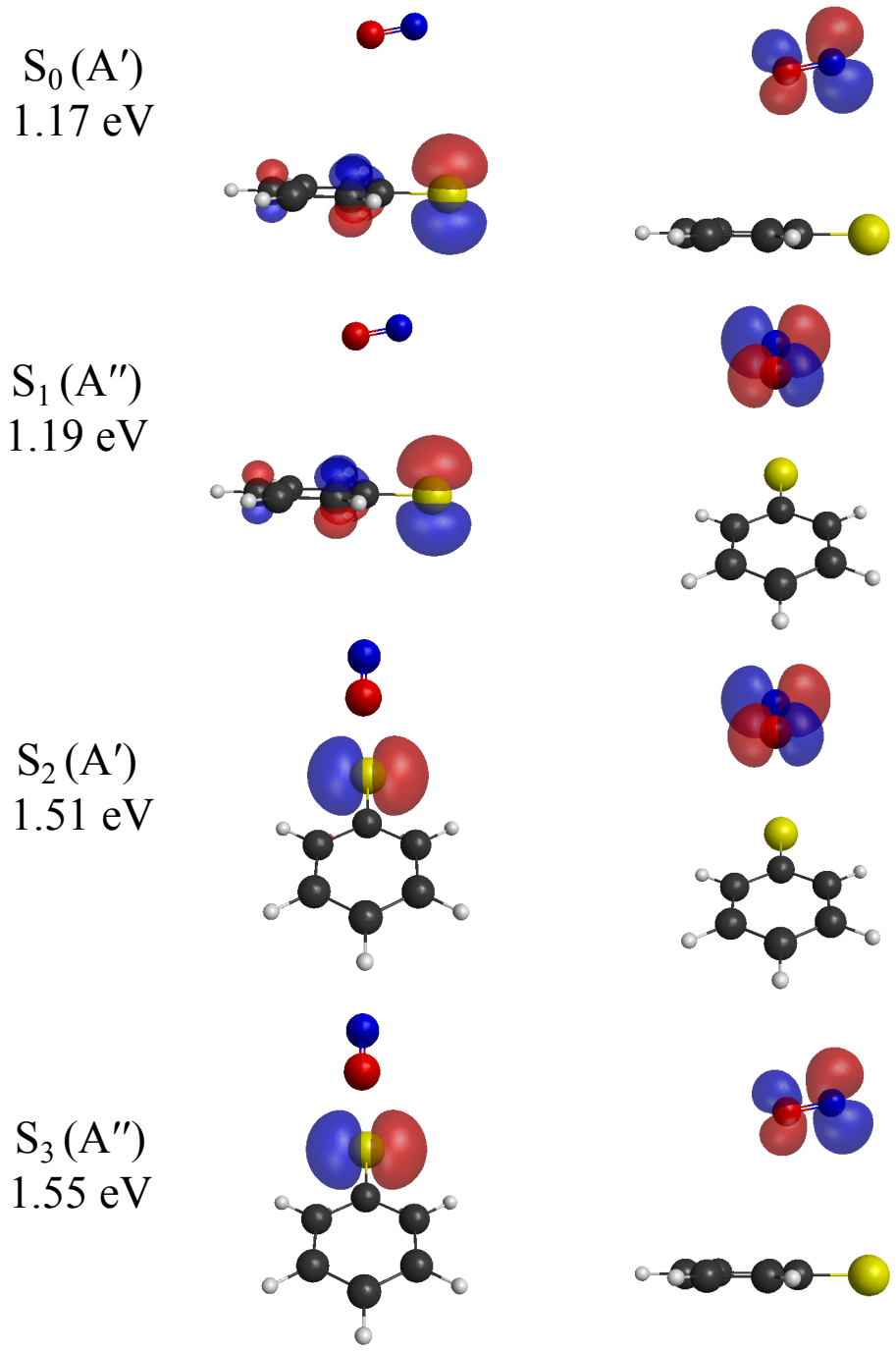

Figure S11: The singly occupied molecular orbitals in the dominant electron configurations of the S_0, S_1, S_2, and S_3 states at the geometry with a 4.40 Å S-N bond length. The energies are reported relative to that of the S_0 state at the optimized geometry of the *syn* conformer.

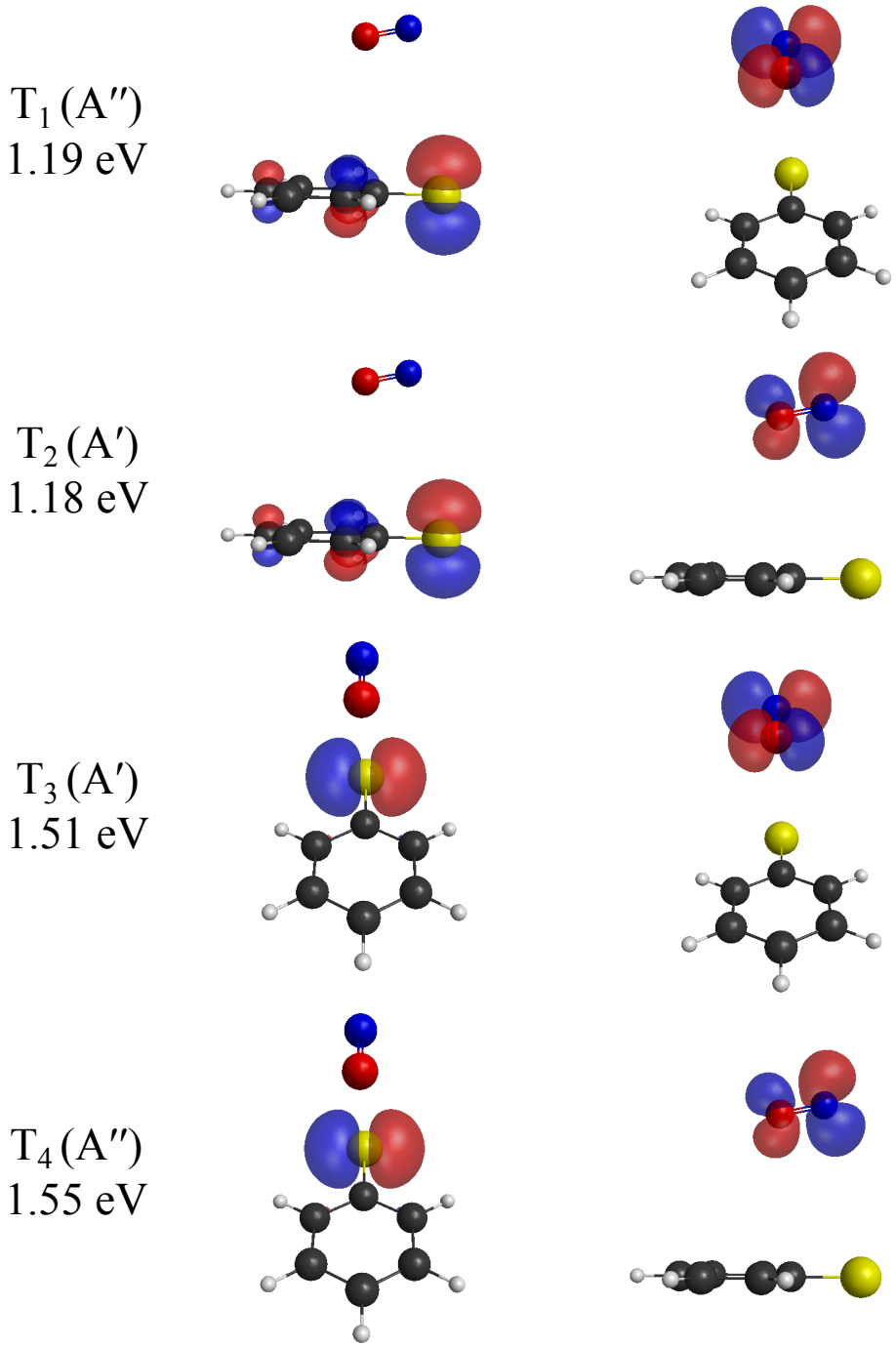

Figure S12: The singly occupied molecular orbitals in the dominant electron configurations of the T_1, T_2, T_3, and T_4 states at the geometry with a 4.40 Å S-N bond length. The energies are reported relative to that of the S_0 state at the optimized geometry of the *syn* conformer.

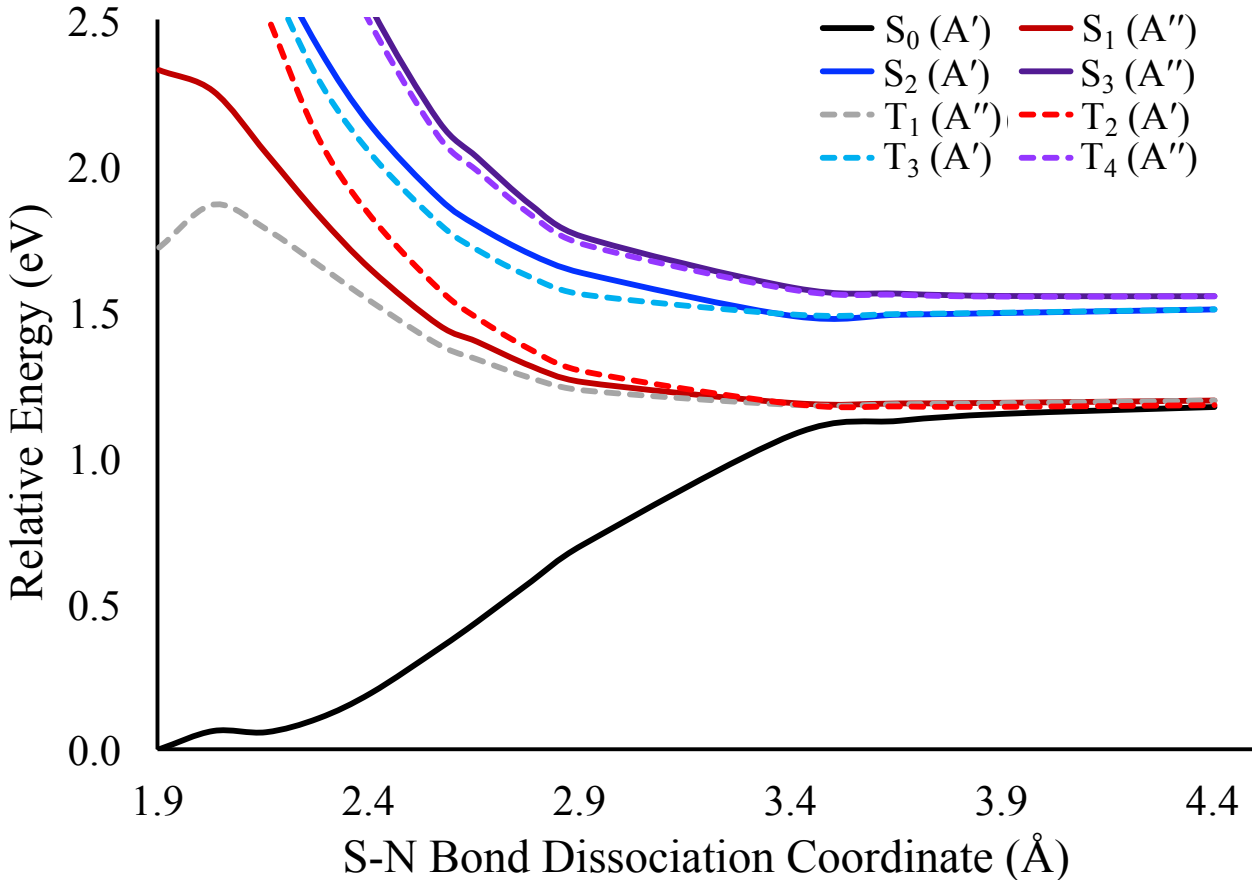

Figure S13: A zoomed in version of Figure 1 in the manuscript showing that at large S-N bond lengths, T_2 approaches the same dissociation limit as S_0. The calculation was performed at the (18,14) MCQDPT2/aug-cc-pvdz level of theory with the lowest three singlet or triplet states of each irreducible representation of the C_s point group state averaged.

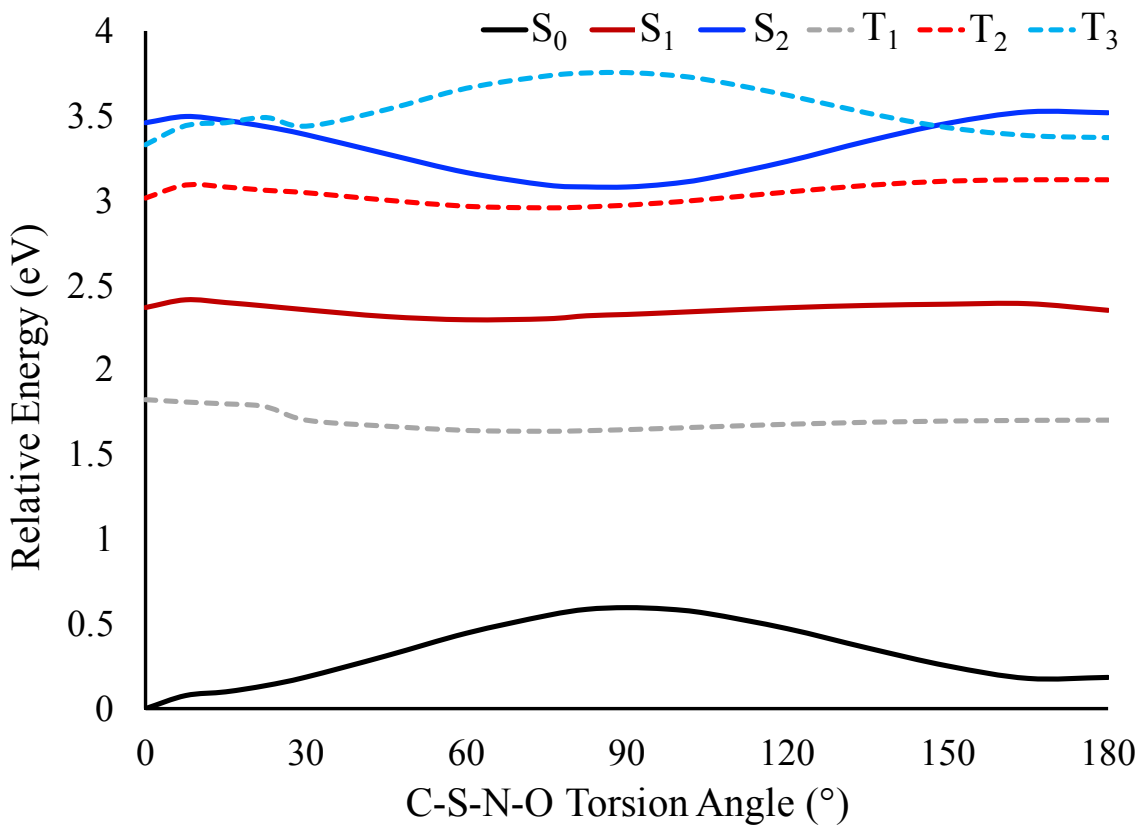

Figure S14: Reproduction of Figure 4 from the manuscript showing an unrelaxed scan along the C-S-N-O torsion angle at $R_{S\text{-}N}$ = 1.9 Å. The calculation was performed at the (16,13) MCQDPT2/aug-cc-pvdz level of theory with state-averaging over the lowest four singlet or triplet states. All energies are reported relative to the lowest S_0 energy in this scan.

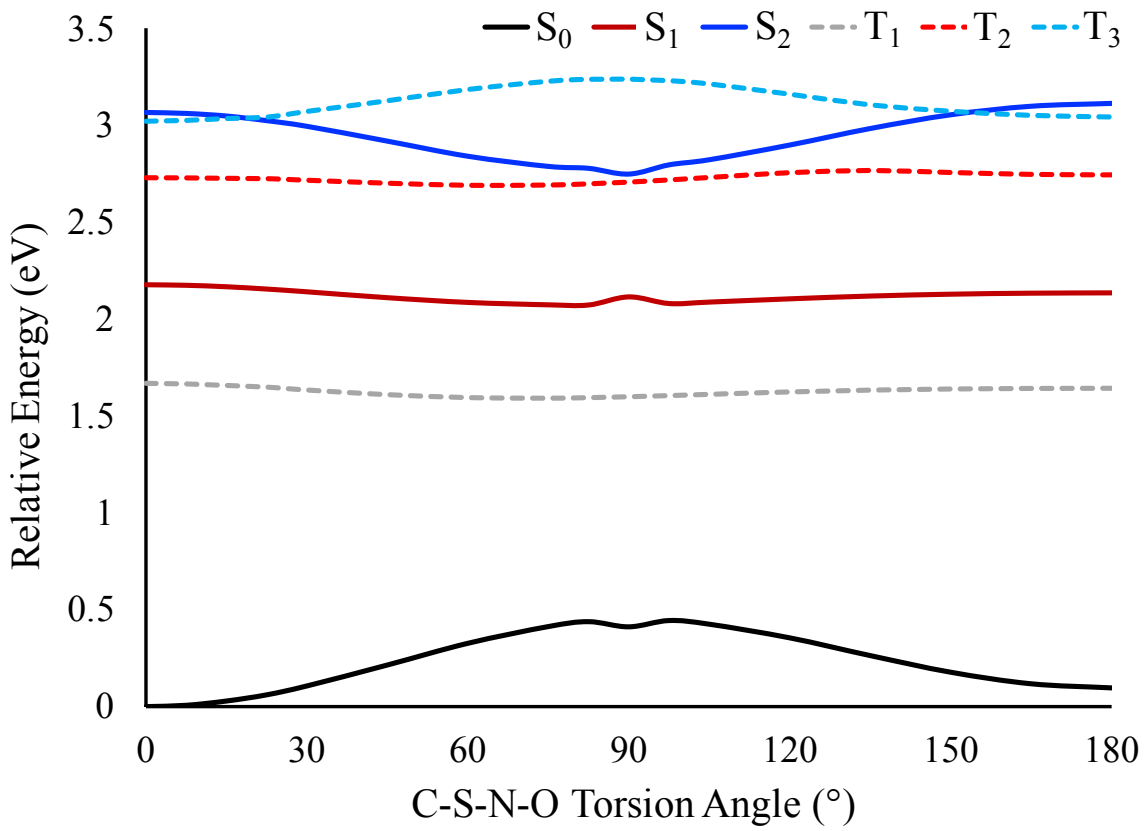

Figure S15: Results from an unrelaxed scan along the C-S-N-O torsion angle at $R_{S\text{-}N}$ = 2.0 Å. The calculation was performed at the (16,13) MCQDPT2/aug-cc-pvdz level of theory with state-averaging over the lowest four singlet or triplet states. All energies are reported relative to the lowest S_0 energy in this scan.

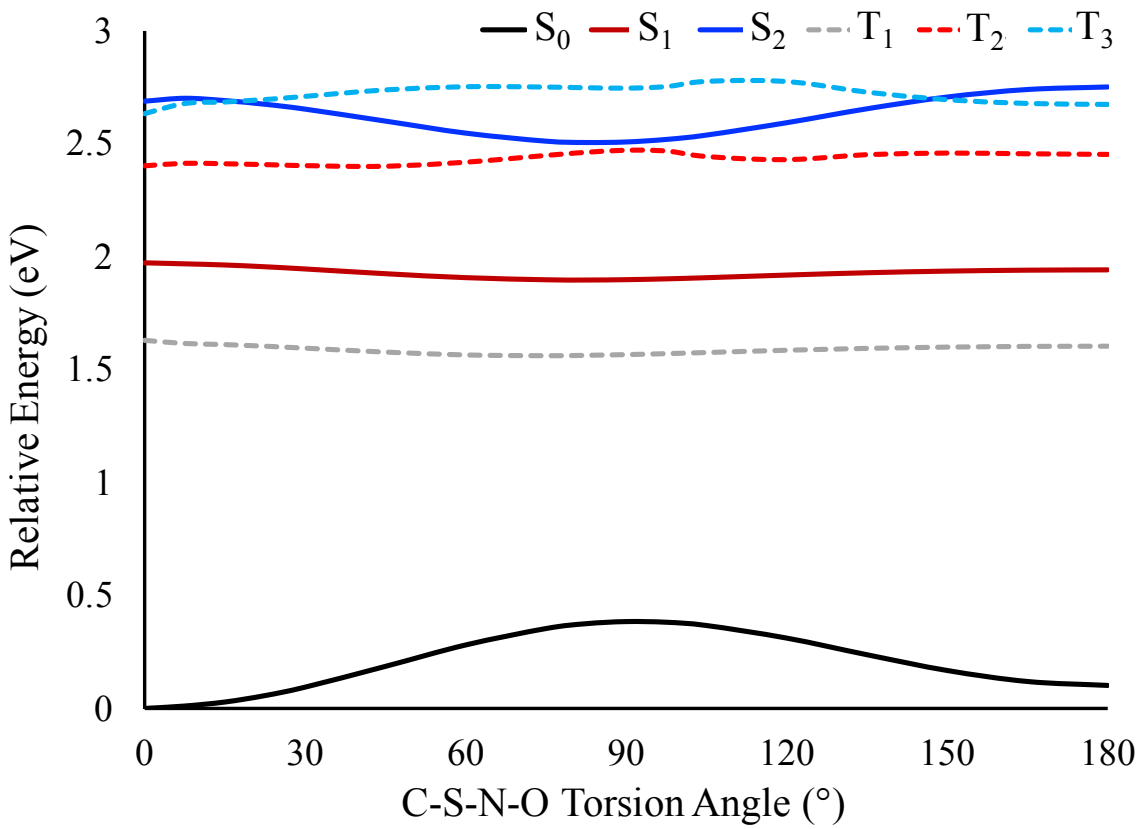

Figure S16: Results from an unrelaxed scan along the C-S-N-O torsion angle at $R_{S\text{-}N}$ = 2.1 Å. The calculation was performed at the (16,13) MCQDPT2/aug-cc-pvdz level of theory with state-averaging over the lowest four singlet or triplet states. All energies are reported relative to the lowest S_0 energy in this scan.

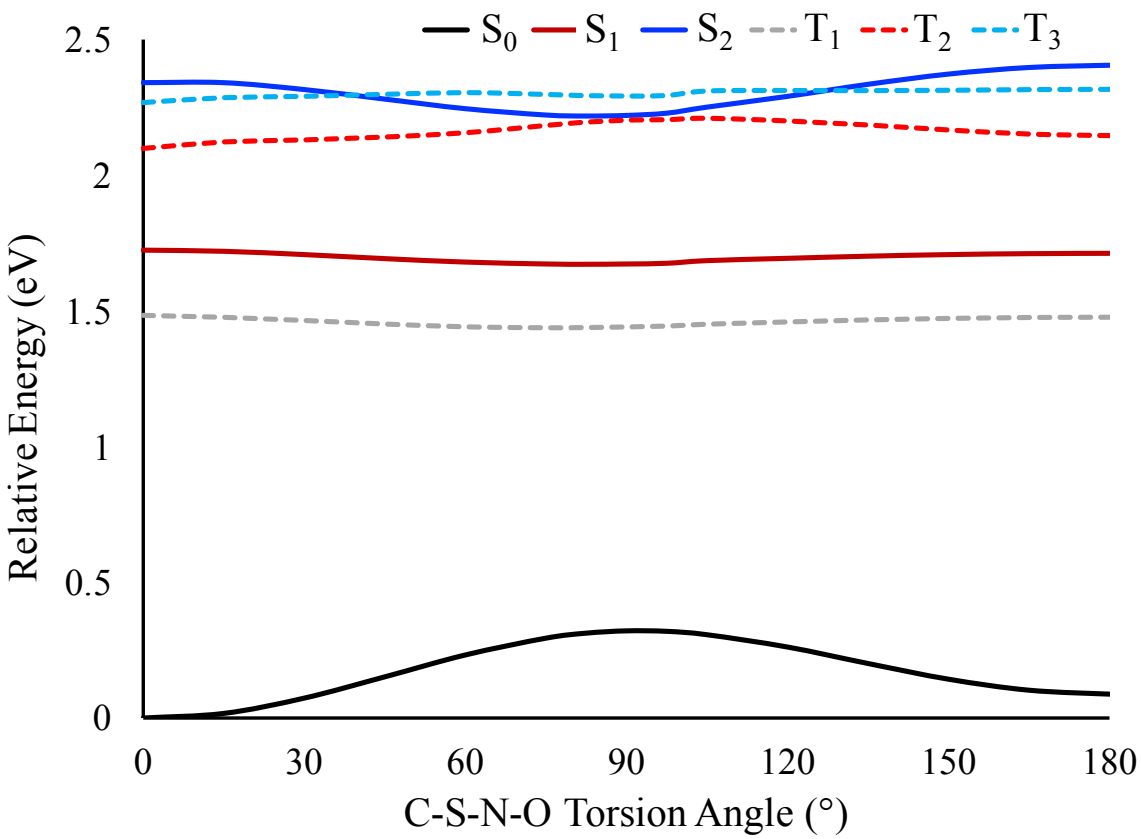

Figure S17: Results from an unrelaxed scan along the C-S-N-O torsion angle at $R_{S\text{-}N}$ = 2.2 Å. The calculation was performed at the (16,13) MCQDPT2/aug-cc-pvdz level of theory with state-averaging over the lowest four singlet or triplet states. All energies are reported relative to the lowest S_0 energy in this scan.

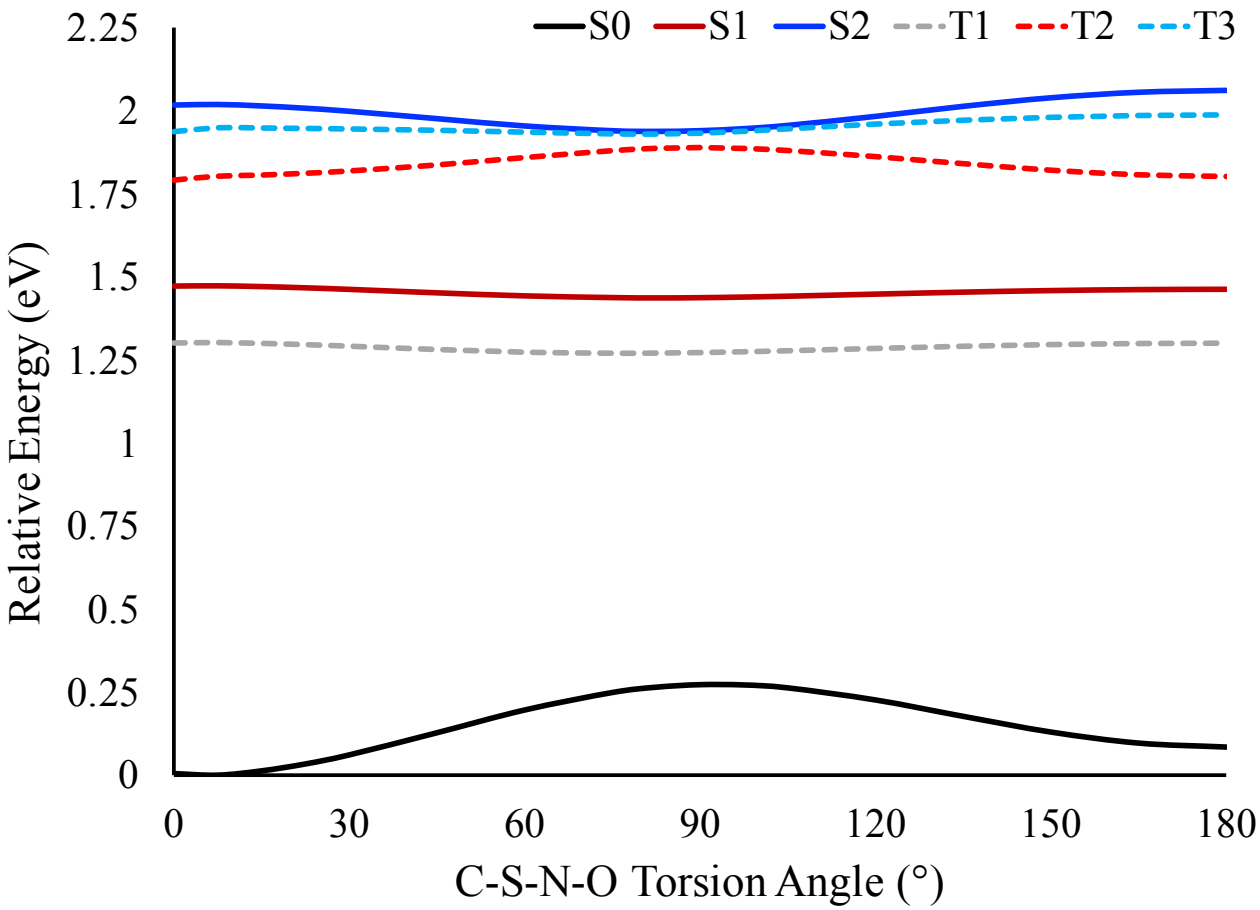

Figure S18: Results from an unrelaxed scan along the C-S-N-O torsion angle at $R_{S\text{-}N}$ = 2.3 Å. The calculation was performed at the (16,13) MCQDPT2/aug-cc-pvdz level of theory with state-averaging over the lowest four singlet or triplet states. All energies are reported relative to the lowest S_0 energy in this scan.

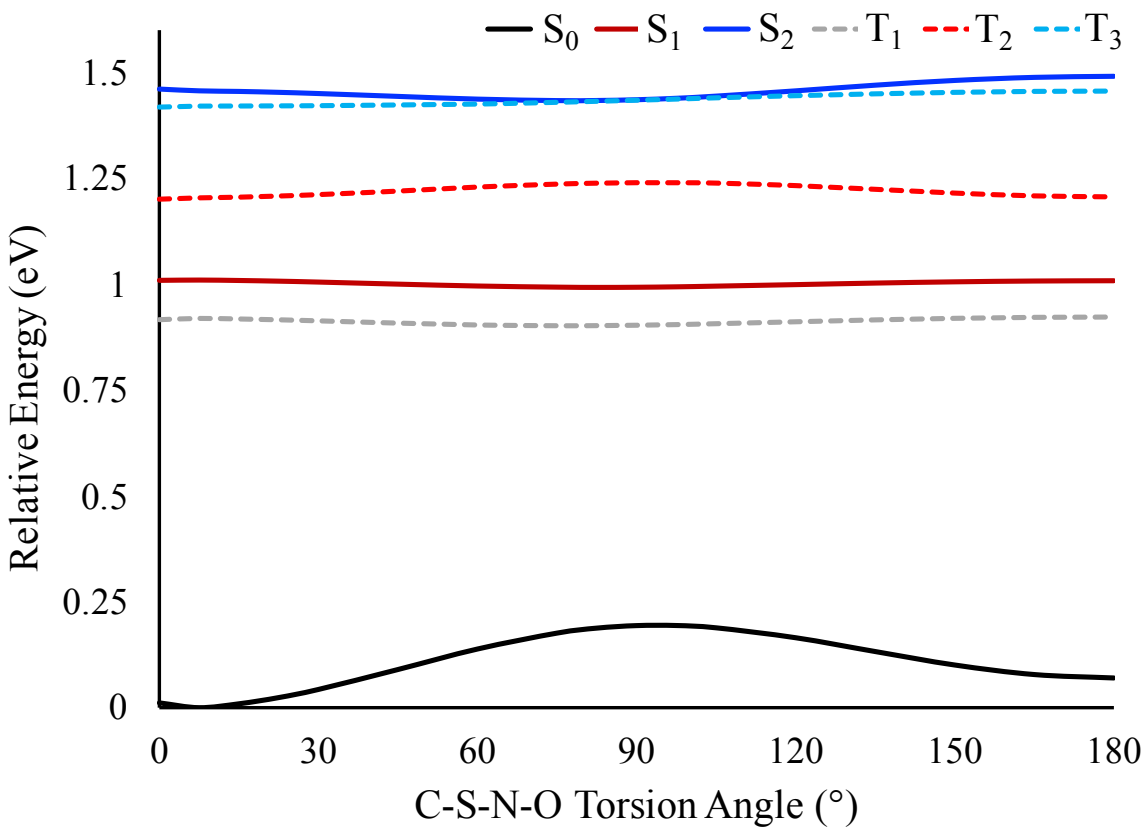

Figure S19: Results from an unrelaxed scan along the C-S-N-O torsion angle at $R_{S\text{-}N}$ = 2.5 Å. The calculation was performed at the (16,13) MCQDPT2/aug-cc-pvdz level of theory with state-averaging over the lowest four singlet or triplet states. All energies are reported relative to the lowest S_0 energy in this scan.

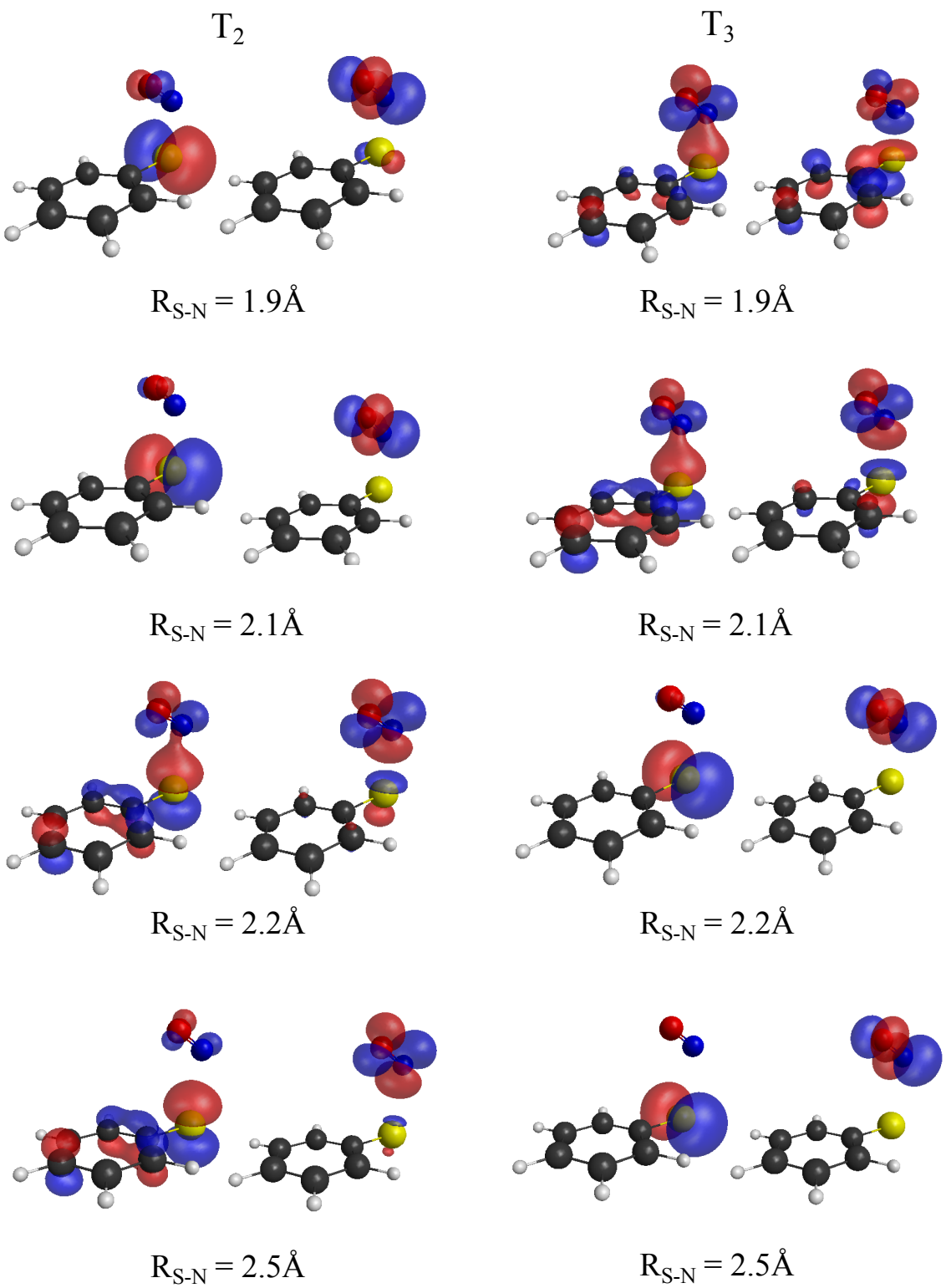

Figure S20: Plots of the singly occupied molecular orbitals of T_2 and T_3 at different values of $R_{S\text{-}N}$ and a C-S-N-O torsion angle of 0º. Note that the electronic characters of the T_2 and T_3 adiabatic states switch between $R_{S\text{-}N}$ = 2.1 Å and $R_{S\text{-}N}$ = 2.3 Å.

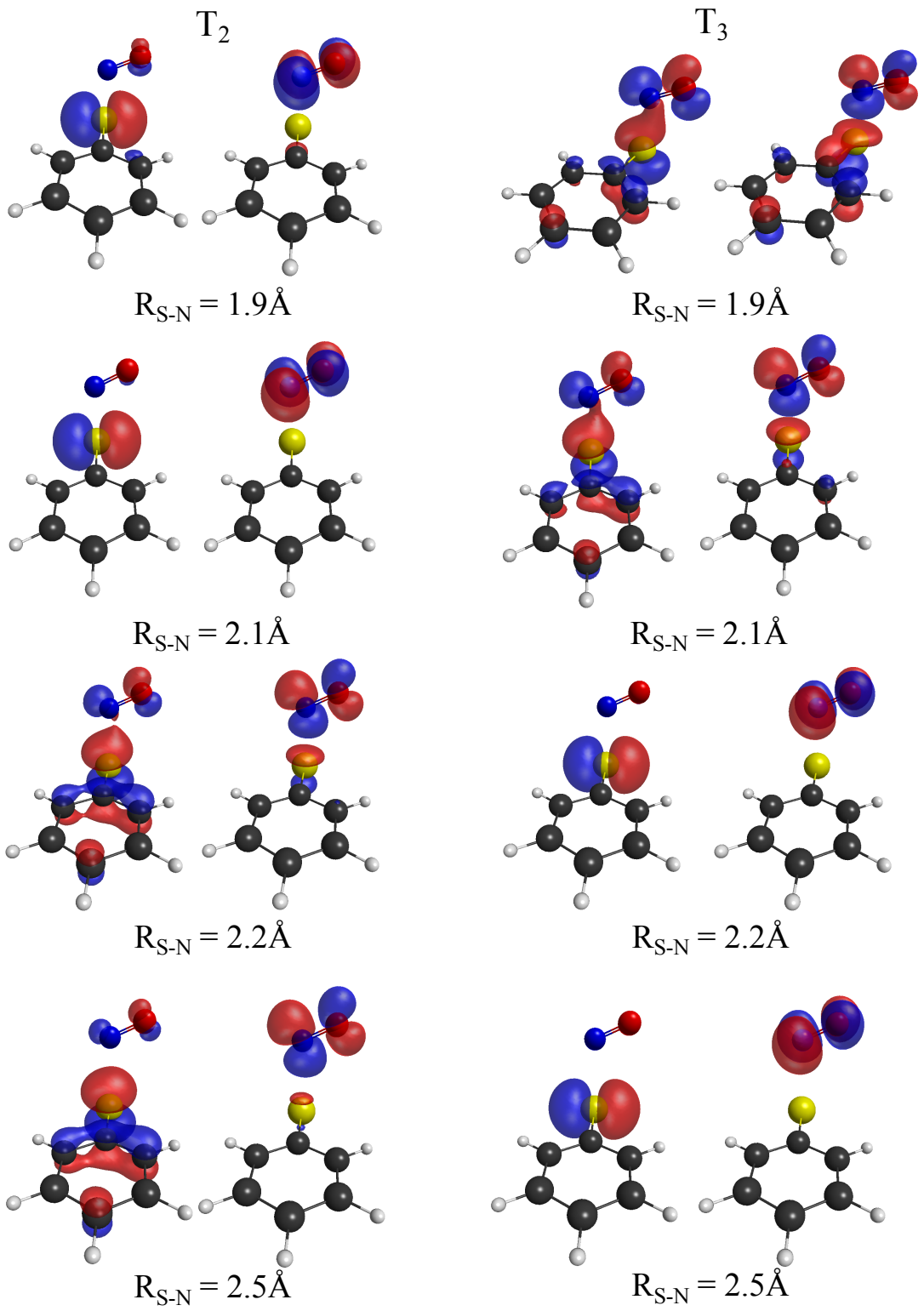

Figure S21: Plots of the singly occupied molecular orbitals of T_2 and T_3 at different values of $R_{S\text{-}N}$ and a C-S-N-O torsion angle of 90º. Note that the electronic characters of the T_2 and T_3 adiabatic states switch between $R_{S\text{-}N}$ = 2.1 Å and $R_{S\text{-}N}$ = 2.3 Å.

Table S1: Relative electronic energies of the singlet states from the relaxed scan along the S-N bond dissociation coordinate used to produce Figures 1 and S6. The calculation was performed at the (18,14) MCQDPT2/aug-cc-pvdz level of theory with the lowest three singlet states of each irreducible representation of the C_s point group state averaged.

S-N Bond Length (Å)	S_0 (eV)	S_1 (eV)	S_2 (eV)	S_3 (eV)
1.90	0.00	2.33	3.43	4.45
2.03	0.06	2.25	3.16	4.07
2.16	0.06	2.04	2.75	3.46
2.28	0.11	1.83	2.40	2.95
2.41	0.19	1.64	2.13	2.54
2.57	0.35	1.45	1.89	2.15
2.66	0.44	1.40	1.79	2.03
2.79	0.58	1.31	1.69	1.86
2.91	0.70	1.26	1.63	1.76
3.16	0.99	1.20	1.49	1.63
3.41	1.08	1.19	1.48	1.58
3.66	1.13	1.18	1.49	1.56
3.91	1.15	1.19	1.49	1.55
4.40	1.17	1.19	1.51	1.55

Table S2: Relative electronic energies of the triplet states from the relaxed scan along the S-N bond dissociation coordinate used to produce Figures 1 and S6. The calculation was performed at the (18,14) MCQDPT2/aug-cc-pvdz level of theory with the lowest three triplet states of each irreducible representation of the C_s point group state averaged.

S-N Bond Length (Å)	T_1 (eV)	T_2 (eV)	T_3 (eV)	T_4 (eV)
1.90	1.72	3.05	3.44	4.30
2.03	1.87	2.94	3.06	3.89
2.16	1.78	2.52	2.66	3.33
2.28	1.66	2.09	2.29	2.85
2.41	1.53	1.82	2.04	2.48
2.57	1.39	1.58	1.80	2.10
2.66	1.34	1.48	1.71	1.98
2.79	1.27	1.37	1.62	1.83
2.91	1.23	1.30	1.56	1.73
3.16	1.19	1.21	1.50	1.62
3.41	1.18	1.18	1.49	1.57
3.66	1.18	1.17	1.49	1.56
3.91	1.19	1.17	1.50	1.55
4.40	1.19	1.18	1.51	1.55

Table S3: Transition dipole moment components (given in percent) of PhSNO calculated at the TD-DFT/6-311+G(d,p) level of theory.

Electronic State	% μ_a	% μ_b	% μ_c
S_1	0	100	0
S_2	7	0	93
S_3	43	0	57

Table S4: Relative electronic energies from the unrelaxed scan along the C-S-N-O torsion angle at R_{SN} = 1.9 Å used to produce Figures 4 and S7. The calculation was performed at the (16,13) MCQDPT2/aug-cc-pvdz level of theory. All energies are reported relative to the lowest S_0 energy in this scan.

C-S-N-O Torsion Angle (°)	S_0 (eV)	S_1 (eV)	S_2 (eV)	T_1 (eV)	T_2 (eV)	T_3 (eV)
0.0	0.00	2.37	3.46	1.82	3.01	3.33
7.5	0.08	2.41	3.50	1.81	3.09	3.44
15.0	0.10	2.40	3.47	1.80	3.08	3.46
22.5	0.14	2.38	3.44	1.78	3.06	3.49
30.0	0.19	2.35	3.39	1.70	3.05	3.44
45.0	0.31	2.31	3.27	1.67	3.00	3.54
60.0	0.45	2.30	3.16	1.64	2.96	3.66
75.0	0.55	2.30	3.09	1.64	2.96	3.73
82.5	0.59	2.32	3.08	1.64	2.96	3.75
90.0	0.60	2.33	3.08	1.65	2.97	3.75
97.5	0.59	2.34	3.10	1.65	2.99	3.74
105.0	0.56	2.35	3.13	1.66	3.01	3.71
120.0	0.47	2.37	3.23	1.68	3.05	3.62
135.0	0.36	2.38	3.35	1.69	3.09	3.52
150.0	0.25	2.39	3.45	1.70	3.11	3.43
165.0	0.18	2.39	3.52	1.70	3.12	3.38
180.0	0.18	2.35	3.52	1.70	3.12	3.37

Table S5: Relative electronic energies from the unrelaxed scan along the C-S-N-O torsion angle at R_{SN} = 2.0 Å used to produce Figure S8. The calculation was performed at the (16,13) MCQDPT2/aug-cc-pvdz level of theory. All energies are reported relative to the lowest S_0 energy in this scan.

C-S-N-O Torsion Angle (°)	S_0 (eV)	S_1 (eV)	S_2 (eV)	T_1 (eV)	T_2 (eV)	T_3 (eV)
0.0	0.00	2.18	3.07	1.67	2.73	3.02
7.5	0.01	2.17	3.06	1.66	2.73	3.02
15.0	0.03	2.17	3.05	1.66	2.73	3.03
22.5	0.06	2.15	3.02	1.65	2.72	3.04
30.0	0.11	2.14	2.99	1.63	2.72	3.07
45.0	0.21	2.11	2.92	1.61	2.70	3.13
60.0	0.33	2.09	2.84	1.59	2.69	3.18
75.0	0.41	2.07	2.79	1.59	2.69	3.23
82.5	0.44	2.07	2.78	1.59	2.70	3.24
90.0	0.41	2.11	2.75	1.60	2.71	3.24
97.5	0.44	2.08	2.80	1.60	2.72	3.23
105.0	0.43	2.09	2.82	1.61	2.73	3.21
120.0	0.35	2.10	2.90	1.62	2.75	3.16
135.0	0.26	2.12	2.98	1.63	2.77	3.10
150.0	0.18	2.13	3.05	1.64	2.76	3.07
165.0	0.12	2.13	3.10	1.64	2.75	3.05
180.0	0.10	2.13	3.11	1.64	2.74	3.04

Table S6: Relative electronic energies from the unrelaxed scan along the C-S-N-O torsion angle at R_{SN} = 2.1 Å used to produce Figure S9. The calculation was performed at the (16,13) MCQDPT2/aug-cc-pvdz level of theory. All energies are reported relative to the lowest S_0 energy in this scan.

C-S-N-O Torsion Angle (°)	S_0 (eV)	S_1 (eV)	S_2 (eV)	T_1 (eV)	T_2 (eV)	T_3 (eV)
0.0	0.00	1.97	2.69	1.63	2.40	2.63
7.5	0.01	1.97	2.70	1.62	2.41	2.68
15.0	0.03	1.96	2.69	1.61	2.41	2.69
22.5	0.06	1.96	2.68	1.60	2.41	2.70
30.0	0.09	1.95	2.65	1.60	2.40	2.71
45.0	0.19	1.93	2.60	1.58	2.40	2.74
60.0	0.28	1.91	2.55	1.57	2.42	2.75
75.0	0.35	1.90	2.51	1.56	2.45	2.75
82.5	0.38	1.90	2.51	1.56	2.46	2.75
90.0	0.38	1.90	2.51	1.57	2.47	2.75
97.5	0.38	1.90	2.52	1.57	2.47	2.75
105.0	0.37	1.91	2.54	1.58	2.44	2.78
120.0	0.31	1.92	2.59	1.59	2.43	2.78
135.0	0.24	1.93	2.66	1.59	2.45	2.73
150.0	0.17	1.94	2.71	1.60	2.46	2.70
165.0	0.12	1.94	2.74	1.60	2.46	2.68
180.0	0.10	1.94	2.75	1.60	2.45	2.67

Table S7: Relative electronic energies from the unrelaxed scan along the C-S-N-O torsion angle at R_{SN} = 2.2 Å used to produce Figure S10. The calculation was performed at the (16,13) MCQDPT2/aug-cc-pvdz level of theory. All energies are reported relative to the lowest S_0 energy in this scan.

C-S-N-O Torsion Angle (°)	S_0 (eV)	S_1 (eV)	S_2 (eV)	T_1 (eV)	T_2 (eV)	T_3 (eV)
0.0	0.00	1.73	2.34	1.49	2.10	2.27
7.5	0.00	1.73	2.36	1.48	2.13	2.30
15.0	0.02	1.72	2.34	1.48	2.12	2.29
22.5	0.04	1.72	2.34	1.48	2.14	2.30
30.0	0.07	1.71	2.32	1.47	2.13	2.29
45.0	0.15	1.69	2.28	1.45	2.14	2.30
60.0	0.23	1.68	2.25	1.44	2.16	2.31
75.0	0.30	1.67	2.22	1.44	2.18	2.30
82.5	0.31	1.67	2.22	1.44	2.20	2.29
90.0	0.32	1.67	2.22	1.44	2.20	2.29
97.5	0.32	1.68	2.23	1.45	2.21	2.29
105.0	0.31	1.69	2.25	1.45	2.21	2.31
120.0	0.26	1.70	2.29	1.46	2.20	2.31
135.0	0.20	1.70	2.34	1.47	2.19	2.31
150.0	0.14	1.71	2.37	1.47	2.17	2.31
165.0	0.10	1.71	2.40	1.48	2.15	2.32
180.0	0.09	1.71	2.41	1.48	2.15	2.32

Table S8: Relative electronic energies from the unrelaxed scan along the C-S-N-O torsion angle at R_{SN} = 2.3 Å used to produce Figure S11. The calculation was performed at the (16,13) MCQDPT2/aug-cc-pvdz level of theory. All energies are reported relative to the lowest S_0 energy in this scan.

C-S-N-O Torsion Angle (°)	S_0 (eV)	S_1 (eV)	S_2 (eV)	T_1 (eV)	T_2 (eV)	T_3 (eV)
0.0	0.00	1.47	2.02	1.30	1.79	1.94
7.5	0.00	1.47	2.02	1.30	1.80	1.95
15.0	0.01	1.47	2.01	1.30	1.81	1.95
22.5	0.03	1.47	2.01	1.30	1.81	1.95
30.0	0.06	1.46	2.00	1.29	1.82	1.94
45.0	0.13	1.45	1.98	1.28	1.84	1.94
60.0	0.20	1.44	1.95	1.27	1.86	1.94
75.0	0.25	1.44	1.94	1.27	1.88	1.93
82.5	0.26	1.44	1.94	1.27	1.89	1.93
90.0	0.27	1.44	1.94	1.27	1.89	1.93
97.5	0.27	1.44	1.95	1.27	1.89	1.94
105.0	0.26	1.44	1.96	1.28	1.88	1.95
120.0	0.23	1.45	1.98	1.28	1.86	1.96
135.0	0.18	1.45	2.01	1.29	1.84	1.97
150.0	0.13	1.46	2.04	1.30	1.82	1.98
165.0	0.10	1.46	2.06	1.30	1.81	1.99
180.0	0.08	1.46	2.06	1.30	1.80	1.99

Table S9: Relative electronic energies from the unrelaxed scan along the C-S-N-O torsion angle at R_{SN} = 2.5 Å used to produce Figure S12. The calculation was performed at the (16,13) MCQDPT2/aug-cc-pvdz level of theory. All energies are reported relative to the lowest S_0 energy in this scan.

C-S-N-O Torsion Angle (°)	S_0 (eV)	S_1 (eV)	S_2 (eV)	T_1 (eV)	T_2 (eV)	T_3 (eV)
0.0	0.01	1.01	1.46	0.92	1.20	1.42
7.5	0.00	1.01	1.46	0.92	1.20	1.42
15.0	0.01	1.01	1.46	0.92	1.21	1.42
22.5	0.02	1.01	1.45	0.92	1.21	1.42
30.0	0.04	1.01	1.45	0.91	1.21	1.42
45.0	0.09	1.00	1.44	0.91	1.22	1.42
60.0	0.14	1.00	1.44	0.90	1.23	1.43
75.0	0.18	0.99	1.43	0.90	1.24	1.43
82.5	0.19	0.99	1.43	0.90	1.24	1.43
90.0	0.19	0.99	1.44	0.90	1.24	1.43
97.5	0.19	0.99	1.44	0.90	1.24	1.44
105.0	0.19	1.00	1.44	0.91	1.24	1.44
120.0	0.17	1.00	1.46	0.91	1.23	1.45
135.0	0.13	1.00	1.47	0.92	1.22	1.45
150.0	0.10	1.01	1.48	0.92	1.22	1.45
165.0	0.08	1.01	1.49	0.92	1.21	1.46
180.0	0.07	1.01	1.49	0.92	1.21	1.46